Surface & Coatings Technology 484 (2024) 130785

Contents lists available at ScienceDirect

Surface & Coatings Technology

journal homepage: www.elsevier.com/locate/surfcoat

Surface-modified graphite felt incorporating synergistic effects of TiO_2 decoration, nitrogen doping, and porous structure for high-performance vanadium redox flow batteries☆

Yu-Sheng Hsiao [a], Jen-Hsien Huang [b], Hong-Yu Lin [b], Wei Kong Pang [c], Min-Tzu Hung [a], Ta-Hung Cheng [a,d], Shih-Chieh Hsu [e,*], Huei Chu Weng [f,*], Yu-Ching Huang [d,*]

[a] Department of Materials Science and Engineering, National Taiwan University of Science and Technology, No. 43, Sec. 4, Keelung Road, Da-an District, Taipei 10607, Taiwan
[b] Department of Green Material Technology, Green Technology Research Institute, CPC Corporation, No.2, Zuonan Rd., Nanzi District, Kaohsiung City, 81126, Taiwan
[c] Faculty of Engineering, Institute for Superconducting & Electronic Materials, University of Wollongong, Wollongong, NSW, Australia
[d] Department of Materials Engineering, Ming Chi University of Technology, 84 Gungjuan Road, Taishan District, New Taipei City, 24301, Taiwan
[e] Department of Chemical and Materials Engineering, Tamkang University, No. 151, Yingzhuan Road, Tamsui District, New Taipei City 25137, Taiwan
[f] Department of Mechanical Engineering, Chung Yuan Christian University, No. 200, Chungpei Road, Chungli District, Taoyuan City 32023, Taiwan

ARTICLE INFO

Keywords:
Redox flow battery
Surface modification
Porous structure
Graphite felt (GF)
Energy storage

ABSTRACT

Construction of porous surface, decoration of metal oxide, and introduction of defects are three major strategies to improve the electrocatalytic capability of graphite felt (GF) for vanadium redox flow battery (VRFB). In this study, we have successfully achieved the urea-assisted deposition of TiO_2 onto GF, resulting in a synergistic effect that realizes the three modifications mentioned above, through a facile one-pot approach. During the post-annealing process, the decorated TiO_2 can further undergo carbon-thermal reduction to etch the GF surface, leading to a porous surface. Additionally, the defective structures such as oxygen defects and nitrogen doping also be can simultaneously incorporated in the modified GF. As a result, the modified GF shows a dramatically improved electrocatalytic capability towards the VO^{2+}/VO_2^+ redox reactions due to better hydrophilicity, larger surface area, and numerous oxygen defects. The VRFB with the modified GF electrode can deliver the coulombic efficiency (CE), voltage efficiency (VE), and energy efficiency (EE) of 95.0, 81.8, and 77.8 %, respectively, at 160 mA/cm^2, which are much better than those of VRFB based on untreated GF.

1. Introduction

As technology advances rapidly and the global population continues to grow, the energy demand becomes a crucial factor in shaping future development. Traditional fossil energy sources have greatly impacted the natural environment; therefore, renewable energy techniques and power grids have become the primary research topics. Energy storage systems play a crucial role in bridging the gap between intermittent power sources and power grids to meet electricity demand. Numerous energy storage systems, including thermal storage, lithium-ion batteries, supercapacitors, and VRFB, have been suggested as effective means to store electricity [1–3]. Among these technologies, the VRFBs can be used for grid energy storage due to their relative bulkiness. The VRFB was first reported by Skyllas-Kazacos et al. [4–6], employing vanadium ions as the redox-active species without cross-contamination of electrolytes. The VRFBs possess several advantages, including flexibility of capacity, extended lifecycle, cost-effectiveness, high efficiency, and safety. They are regarded as an effective solution for stabilizing the power output in large-scale deployments of electricity from various energy sources.

Typical VRFB cells comprise the redox couples V^{2+}/V^{3+} and VO^{2+}/VO_2^+ redox couples dissolved in a dilute acid solution. Two electrolyte reservoirs are pumped into an electrochemical cell with a continuous circulation to facilitate redox reactions at the corresponding electrodes. Each VRFB cell is composed of an anode, cathode, and ion exchange membrane to facilitate ion diffusion and prevent contamination between the two electrolyte reservoirs. The electrodes are the critical

☆ Special Issue of TACT2023 (Registration No.: 14810268/Abstract No.: A-P-168)

* Corresponding authors.
E-mail addresses: 137422@o365.tku.edu.tw (S.-C. Hsu), hcweng@cycu.edu.tw (H.C. Weng), huangyc@mail.mcut.edu.tw (Y.-C. Huang).

https://doi.org/10.1016/j.surfcoat.2024.130785
Received 6 December 2023; Received in revised form 9 April 2024; Accepted 10 April 2024
Available online 16 April 2024

component to determine the overall performance of VRFBs. Currently, graphite felts (GFs) are extensively utilized as electrode materials in VRFBs due to their excellent stability, large operation potential range, and high conductivity in concentrated acidic environments [7]. Unfortunately, the low catalytic activity, poor wettability, and insufficient surface area of GF limit the mass transport and redox reaction leading to poor energy efficiency. Various strategies, such as thermal/acid treatment, surface modification, nanostructuring, and element doping [8–15], have been proposed to address these limitations. For instance, Y. C. Chang et al. discovered that thermal and acid treatments of GFs can increase the presence of oxygen-containing functional groups, thereby facilitating the redox reactions of vanadium ions [16]. Kabtamu et al. modified the GF surface through a hydrothermal process with niobium-doped hexagonal tungsten trioxide nanowires (Nb-doped h-WO_3 NWs) [17]. The decorated Nb-doped h-WO_3 NWs can enhance the electrocatalytic activity for the redox reaction, thereby improving the energy storage performance. D. S. Yang et al. developed a hierarchically porous GF electrode, which substantially enhances wettability and surface area, facilitating rapid mass transport [18]. The VRFB cell based on the porous GF electrodes yielded an excellent energy efficiency (EE) of around 80 % at a current density of 100 mA/cm^2, which outperformed those of untreated GF electrodes (around 71 %). Recently, J. Ji et al. also prepared nitrogen-doped GF electrodes (SC/U-GF) featuring a microporous structure [19]. The nitrogen-doped SC/U-GF electrodes exhibit reduced electrochemical polarization attributed to the lower charge transfer resistance. The EE of VRFB based on SC/U-GF electrode is 80.2 % at 120 mA cm^{-2}, which is 7.8 % better than that of pristine GF electrodes. The VRFB also reveals excellent cycling stability with a retention of 99.6 % after 300 cycles.

An ideal VRFB electrode is considered to have high electrocatalytic activity, great hydrophilicity, large surface area, and high conductivity to achieve high-performance VRFB. However, it is still challenging to synthesize the electrode materials with the above properties in a single preparation process. Here, we proposed a facile one-pot synthetic strategy to prepare the nitrogen-doped and TiO_2 decorated GF electrode with a hierarchically porous surface. The modified GF electrodes with a synergistic effect of surface modification, nanostructuring, and incorporation of oxygen defects and nitrogen doping reveal improved wettability, catalytic activity, and mass transportation. As a result, the VRFB incorporated the modified GF can deliver an EE of 83.3 % at a current density of 100 mA/cm^2, which was higher than that of pristine GF (78.5 %).

2. Experimental section

2.1. Synthesis of modified GFs

In a typical synthesis process, 2 mL of titanium butoxide (TBT) was dissolved in 60 mL of ethanol. Then, 0.5 g of urea dissolved in deionized water (20 mL) was added to the above TBT solution. Consequently, the commercial GFs (UBIQ TECHNOLOGY Co., Ltd) with a size of 2 × 2 cm^2 were immersed in the mixture under magnetic stirring. After stirring for 2 h, the GFs were then dried at 60 °C overnight to remove the solvent. Finally, the resultant samples were annealed in an N_2 atmosphere at 400 °C for 0.5 h and then heated at 800 °C for 2 h with a heating rate of 10 °C/min to obtain the modified GF. Here, we also prepared the modified GFs with different urea concentrations. The modified GFs prepared with 0.5, 1.5, and 2.5 g of urea are denoted herein as GF-0.5, GF-1.5, and GF-2.5, respectively.

2.2. Characterization

X-ray powder diffraction (XRD) patterns were recorded using a Bruker AXS D8 Advance Eco and Cu Kα radiation (λ = 1.540 Å). Thermogravimetric analysis (TGA, METTLER TOLEDO, STAR system) was performed to study the chemical composition of the composites under air flow with a heating rate of 10 °C/min, from room temperature to 1000 °C. The morphologies of the prepared samples were observed using scanning electron microscopy (SEM, JEOLJSM 6701F). Raman spectra were recorded using a WITEC confocal spectrometer equipped with a grating (600 lines/mm), with excitation at 514.5 nm. The functional groups of the modified GF were characterized by Fourier transform infrared spectroscopy (FTIR, VERTEX70, Bruker, Germany). X-ray photoelectron spectroscopy (XPS) was performed using an ESCALAB 250Xi spectrometer and Al K radiation. Nitrogen sorption isotherms were determined using a Micromeritics Gemini VII 2390 Surface Area Analyzer. All the electrochemical characterizations were measured with an electrochemical workstation (PAR, PARSTAT 4000A).

2.3. VRFB single-cell test

The commercial VRFB single cell used in this study was purchased from C-Tech Innovation (C-Flow 1 × 1 Electrochemical Cell). The electrolyte with a total vanadium concentration of 1.6 M (50 % VO^{2+} and 50 % V^{3+}) in 2 M H_2SO_4 (Plum-Monix Industry Co., Ltd.) was fed with a flow rate of 20 mL/min. The electrolyte volumes were 50 mL and the working area of the GF electrodes on both sides was 1 × 1 cm^2. The charge–discharge curves were collected with a potentiostat/galvanostat (PAR, PARSTAT 4000A).

3. Results and discussion

In this study, we modified the commercial GF by the urea-assisted decoration of TiO_2 particles, followed by thermal annealing in nitrogen ambient. Fig. 1a illustrates the synthetic route towards the TiO_2 decorated nitrogen-doped GF with porous structure for efficient VRFB electrodes. The commercial GF, TBT, and urea were mixed in ethanol/deionized water with vigorous stirring for 2 h. Then, the GF was dried at 60 °C followed by thermal annealing at 800 °C in a nitrogen atmosphere. During the thermal treatment, the Ti precursors were converted into TiO_2 particles and some portion of the TiO_2 particles underwent carbon-thermal reduction [20,21] by the following reaction [22]:

$$TiO_2 + C \rightarrow TiO + COTiO2 + C \rightarrow TiO + CO \quad (1)$$

This procedure consumes the carbon species on the GF leading to a porous surface and the TiO_2 can be partially reduced to a lower valence state. Here, the simple one-step strategy to modify the GF offered a few advantages. First, the decorated TiO_2 particles can improve the wettability characteristics of GF leading to better mass transport between the vanadium active species and electrode. Second, the electrocatalytic activity for the V^{4+}/V^{5+} redox reaction of GF can be enhanced due to the nitrogen doping effect using urea as a doping source. In addition, the surface hydrophilicity of the GF also can be increased by the nitrogen doping, facilitating the contact between the electrolyte ions and the GF electrodes [23,24]. Third, the porous surface of GF created from the carbon-thermal reduction can provide a larger electrochemical interface for improved electrochemical activity, facilitating kinetics and durability for VRFB. The XRD patterns of pristine and modified GF with various urea contents are shown in Fig. 1b. The pristine GF reveals two pronounced XRD peaks located at 26.5 and 43.6°, corresponding to the (002) and (100) planes of graphite [25]. The diffraction intensity of the two peaks dramatically decreases after modification, indicating the formation of structural defects during the annealing process. The XRD patterns of modified GF are compared in Fig. 1c. The rutile TiO_2 particles coexisting with the minor anatase phase can be observed in all modified GFs, indicating the successful modification. TGA was then performed on the modified GF to quantitatively analyze the amount of decorated TiO_2 particles as shown in Fig. 1d. The weight loss of pristine GF occurs at around 640 °C and the residual content of ash is found to be 1.72 % after heating at 1000 °C. In addition, the final weights of GF-0.5, GF-1.5, and GF-2.5 are 8.41, 12.98 and 20.89 %, suggesting that the corresponding contents of deposited TiO_2 on the three samples are 6.69, 11.26 and

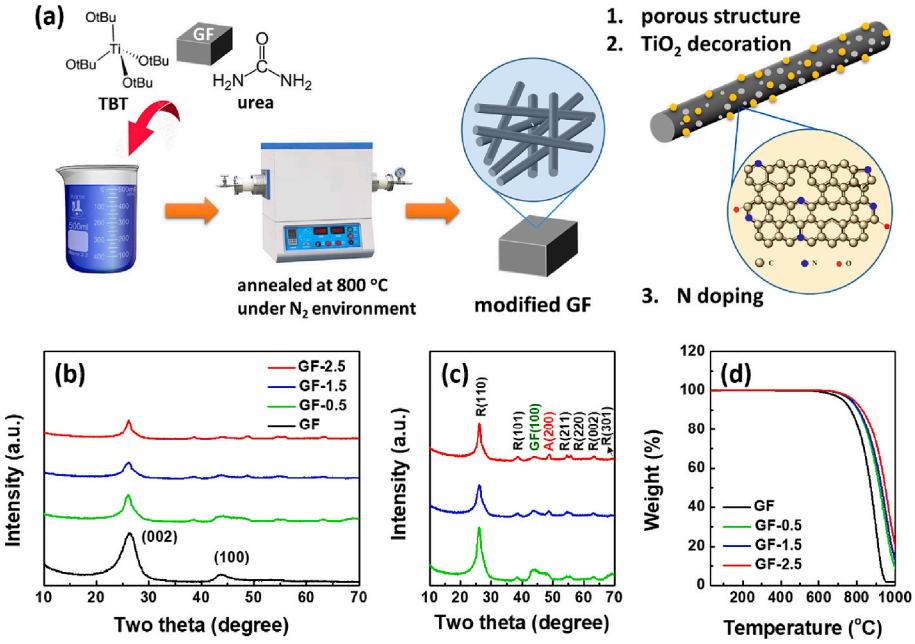

Fig. 1. The synthesis of modified GF. (a) Schematic illustration of the synthetic route of TiO_2 decorated nitrogen doped GF with porous structure; (b) XRD patterns of pristine GF, GF-0.5, GF-1.5, and GF-2.5; (c) XRD patterns of the modified GFs and (d) TGA profile of the four samples.

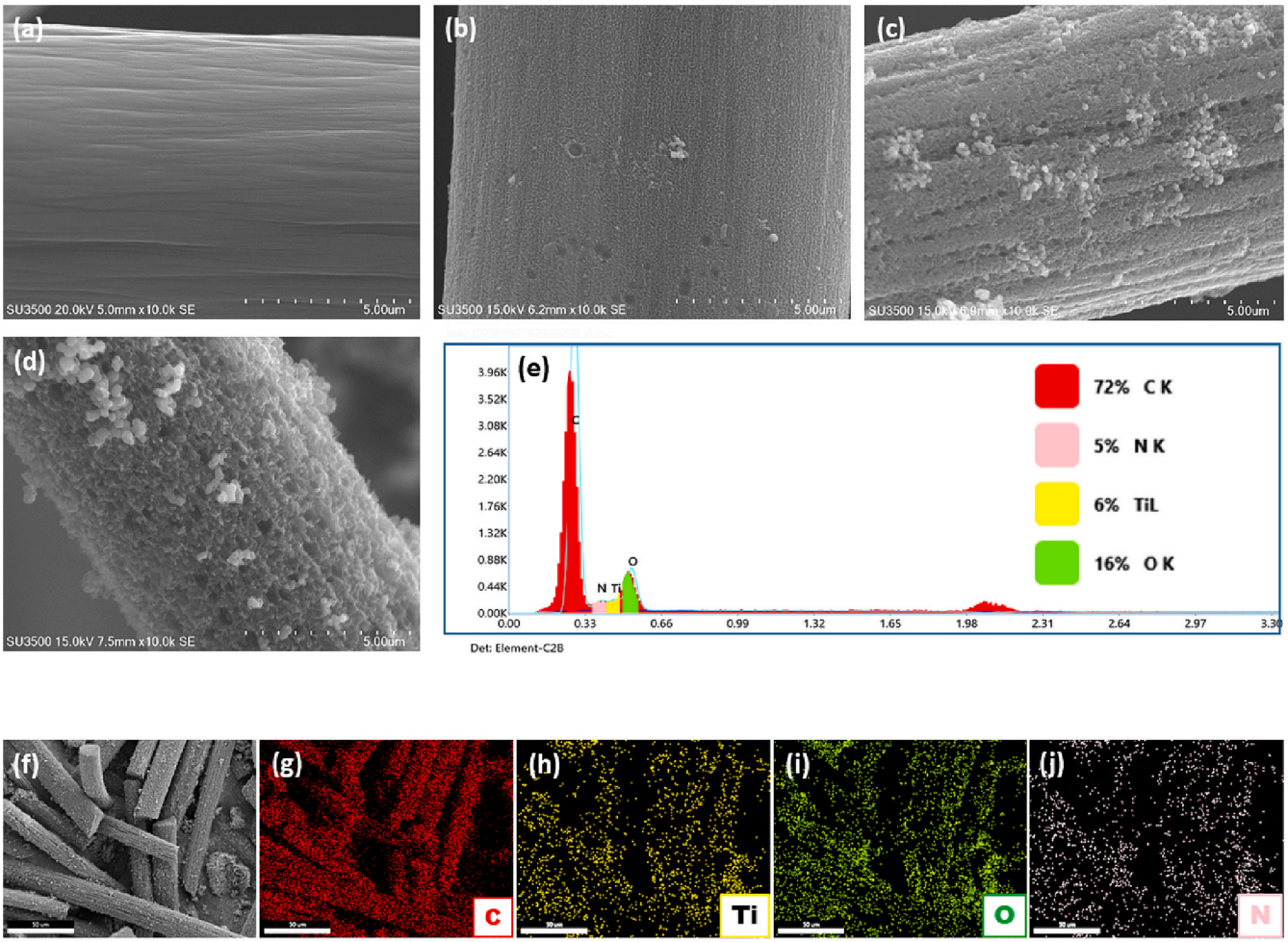

Fig. 2. The morphological investigation of the modified GF. The SEM image of (a) pristine GF; (b) GF-0.5; (c) GF-1.5; (d) GF-2.5; (e) the EDS spectrum of the GF-2.5; (f) the low-magnification SEM image of GF-2.5 and the EDS mapping collected from panel f for (g) C element; (h) Ti element; (i) O element and (j) N element.

19.17 %, respectively.

The surface morphology of these GFs was monitored by SEM observation as shown in Fig. 2. The original GF revealed smooth surface with a diameter of around 10 μm (Fig. 2a). The featureless morphology of the pristine GF results in insufficient interfacial area for mass transfer between the electrolyte and GF electrode. After thermal treatment, it can be seen that a rougher surface with numerous tiny TiO_2 particles evenly and densely distributed on the GF-0.5 surface (Fig. 2b). As the urea content is raised from 0.5 g to 1.5 g, the GF-1.5 surface starts to exhibit a discernible porous structure along with the presence of TiO_2 crystals (Fig. 2c). With further increase in urea content, both the particle size of TiO_2 crystals and the size of surface pores also grow larger. As a result, many nano and sub-micropores with numerous TiO_2 particles are entirely covered on the GF-2.5 surface (Fig. 2d). It has been reported that the urea can serve as a growth enhancer for the synthesis of TiO_2 particles [26]. When urea is dissolved in ethanol solvent, it can easily react with water to produce NH_4OH leading to NH_4^+ and OH^- with increasing the pH value of the solution. The generated OH^- can further hydrolyze Ti^{4+} derived from the TTIP, which can facilitate the formation of TiO_2 crystals [27]. During the post-annealing process, these decorated TiO_2 particles on the GF surface can further experience a carbon-thermal reduction to consume the carbon species and create a porous surface. The detailed mechanism can clarify how our modified GFs not only display increased porosity but also show a much deposition of TiO_2 particles on the surface as the urea content increases. The same results also can be observed in the TGA results as shown in Fig. 1d. It is believed that the porous structure with TiO_2 decoration on the GF can greatly increase the surface area and hydrophilicity of the GF leading to an improved electrochemical performance. In addition, EDS was used to identify the chemical compositions of the GF-2.5 as shown in Fig. 2e, from which it can be seen that GF-2.5 includes the elements of C, Ti, O, and N. The low magnification SEM of GF-2.5 and the corresponding EDS mappings are shown in Fig. 2f–j. The elemental mappings show that the Ti, O, and N elements are uniformly distributed in the sample. These results verify that the GF-2.5 is not only successfully modified with TiO_2 but also doped with nitrogen.

The pristine and modified GF with various urea contents were characterized by the Raman spectrum to further explore the structural information. The Raman spectra of these samples below 1000 cm^{-1}, as shown in Fig. 3a, indicate that no characteristic bands can be found in pristine GF. In contrast, all the modified samples reveal nine pronounced Raman bands. The Raman bands at 194/635, 394, and 513 cm^{-1} observed in GF-2.5 can be assigned to the symmetries E_g, B_{1g}, and A_{1g}/B_{1g} modes in anatase TiO_2, respectively [28,29]. On the other hand, the rutile TiO_2 with stretching Raman bands at 142, 239, 319, 443, and 807 cm^{-1} corresponded to the symmetries of B_{1g}, E_g, A_{1g} and R_{2g} also can be observed in the modified GF, indicating the decorated TiO_2 on GF with rutile/anatase mixed phases [29,30]. Moreover, with the increase in urea content during sample preparation, the intensity of these Raman bands also becomes stronger, implying that the addition of urea indeed improves the formation and growth of TiO_2 crystals. These results are in good agreement with the findings in TGA and SEM measurements. The Raman spectra of these samples between 1000 and 3000 cm^{-1} are also displayed in Fig. 3b. Three typical peaks for the GF can be seen, the D band at 1349 cm^{-1}, the G band at 1586 cm^{-1} and 2D band at 2695 cm^{-1}. The modified GF reveals a larger intensity ratio between the D peak and the G peak (I_D/I_G) compared with that of the pristine one. In addition, as the urea content increases, the I_D/I_G ratio of the sample also rises and the I_D/I_G ratio increases from 1.26 for pristine GF to 1.48 for GF-2.5. These results suggest that defects and disordered structures are introduced, resulting in a lower degree of graphitization during the carbon-thermal etching process [31]. Fig. 3c presents the FTIR spectra of the four samples. The broad peaks located at 515 and 618 cm^{-1} of GF-2.5 can be assigned to Ti–O–Ti stretching modes [32]. The peaks at 1400 and 1632 cm^{-1} are attributed to bending O—H vibration and stretching carboxylic C═O vibrations, respectively [33]. Besides, the C—H stretching modes in the CH_2 and CH_3 groups at 2851 and 2922 cm^{-1} and O—H stretching vibration at 3460 cm^{-1} also can be observed in the FTIR spectrum of GF-2.5 [34]. The nitrogen adsorption-desorption isotherms of the four samples are exhibited in Fig. 3d to evaluate the effect of the created porosity on the surface area. The specific surface area of GF, GF-0.5, GF-1.5, and GF-2.5 based on Fig. 3d is calculated to be 0.41, 3.34, 5.95, and 6.83 m^2/g, thus confirming the higher surface area of GF-2.5 than that of pristine one. The porous structure with a relatively higher surface area aids in lowering resistance for the mass transport of electrolytes during the charge/discharge process, resulting in faster electrochemical kinetics. The pore size distribution of the four samples is also provided in Fig. S1.

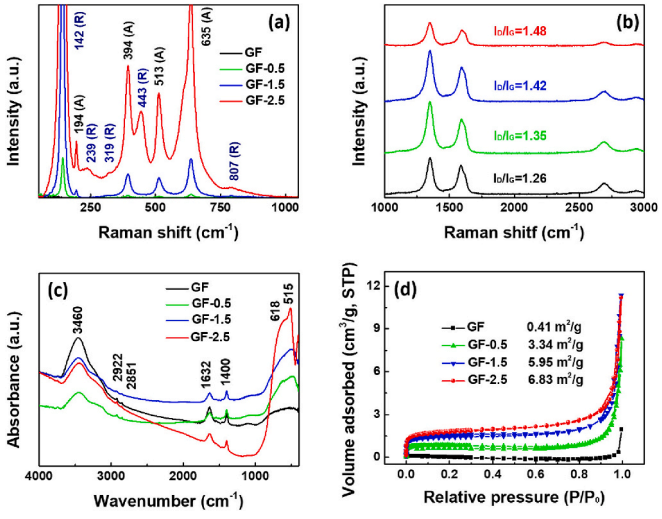

Fig. 3. Spectroscopy analyses of the modified GF. (a, b) Raman spectra of the pristine and modified GF; (c) FTIR spectra of the pristine and modified GF and (d) the nitrogen adsorption-desorption isotherms of the four samples.

The functional groups and chemical states of modified GF were confirmed using XPS analysis. The deconvoluted C1s spectra of GF and GF-2.5 are compared as shown in Fig. 4a, b. Three deconvoluted peaks belonging to C═C, C—C, and C—O can be observed in GF. Except for the three peaks, GF-2.5 displays an additional peak associated with the carboxyl group (O=C-O) [35]. The total oxygen-containing functional groups increase after the modification process, implying that some defects have been introduced in GF-2.5. To conduct a more detailed examination of the composition of oxygen functional groups, the O1s spectra of pristine GF and GF-2.5 were also deconvoluted as shown in Fig. 4c and d. Pristine GF only shows a single peak at 532.5 eV corresponding to either -OH or C—O group [36]. However, in the O 1 s spectrum of GF-2.5, two additional peaks at 532.1 and 530.5 eV are evident, which are related to the O=C-O [37] and Ti—O bonding. This observation confirms the successful incorporation of TiO_2 particles. The N1s and Ti 2p XPS spectra of the GF-2.5 are exhibited as shown in Fig. 4e and f, respectively. The N1s spectrum deconvolution reveals the presence of three distinct nitrogen oxidation states, graphitic, pyrrolic, and pyridinic N, implying that the GF underwent nitrogen doping during the thermal treatment [38,39]. Furthermore, the Ti 2p spectrum of GF-2.5 clearly shows the mixed Ti^{3+}/Ti^{4+} valence state, indicating the partial reduction of Ti^{4+} ions during the carbon-thermal reduction [22,40]. It has been reported that the partial reduction of Ti^{4+} ions during the thermal treatment can induce the generation of oxygen vacancies in TiO_2 leading to higher electronic conductivity [40,41]. The XPS survey of GF-2.5 is also provided in Fig. S2. These modifications to introduce surface defects, nitrogen doping, and TiO_2 decoration can provide an adequate number of reaction sites, better conductivity, and wettability for vanadium redox reaction [42–44]. The XPS results of GF-0.5 and GF-1.5 are also provided in Fig. S3.

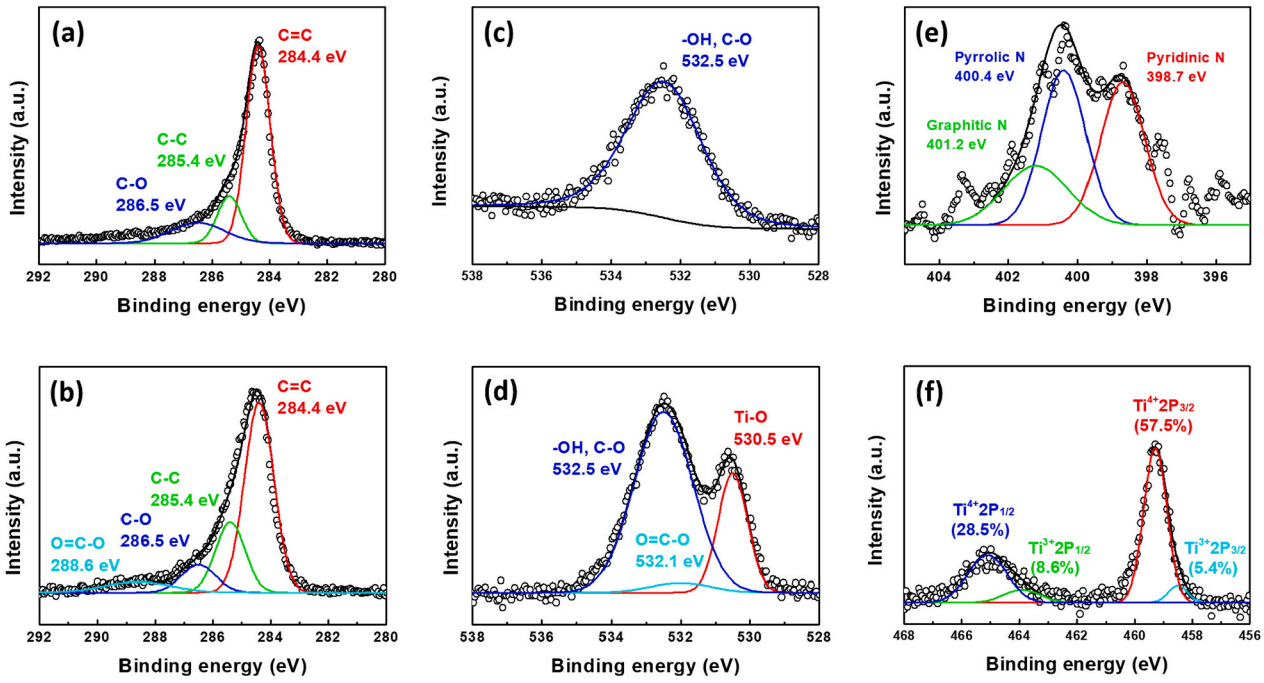

Fig. 4. The investigation of the functional group and chemical state of the modified GF. The peak deconvolution of the C1s XPS spectrum of (a) pristine GF and (b) GF-2.5; The peak deconvolution of the O1s XPS spectrum of (c) pristine GF and (d) GF-2.5; the peak deconvolution of (e) the N1s and (f) Ti2p XPS spectra of GF-2.5.

Fig. 5a shows the CV curves of the pristine and modified GF tested in 1.0 M H_2SO_4 electrolyte with a scan rate of 1 mV/s. It can be seen that the modified samples reveal a nearly rectangular CV shape, indicating the typical electrical double-layer capacitive behavior. With increasing the content of urea, the CV area of the resultant modified GF becomes larger, implying greater capacitance. This originated from the porous structure of the modified GF which can offer a huge electrode/electrolyte interface for the accumulation of electrostatic charge. The CV results further confirm the highly porous structure of GF-2.5. The wettability of these samples was characterized by measuring the water contact angle as shown in Fig. 5b. The pristine GF shows a hydrophobic surface with a contact angle of 126.5°. After the modification, the contact angle significantly decreases due to the creation of oxygen defects and the decoration of hydrophilic TiO_2, which can facilitate electrolyte penetration and ionic migration. The sheet resistance of the four samples is presented in Fig. 5c. Based on the increase in the I_D/I_G ratio after the thermal treatment (Fig. 3b), the electrical conductivity of the modified GF is supposed to decrease due to the formation of structural defects.

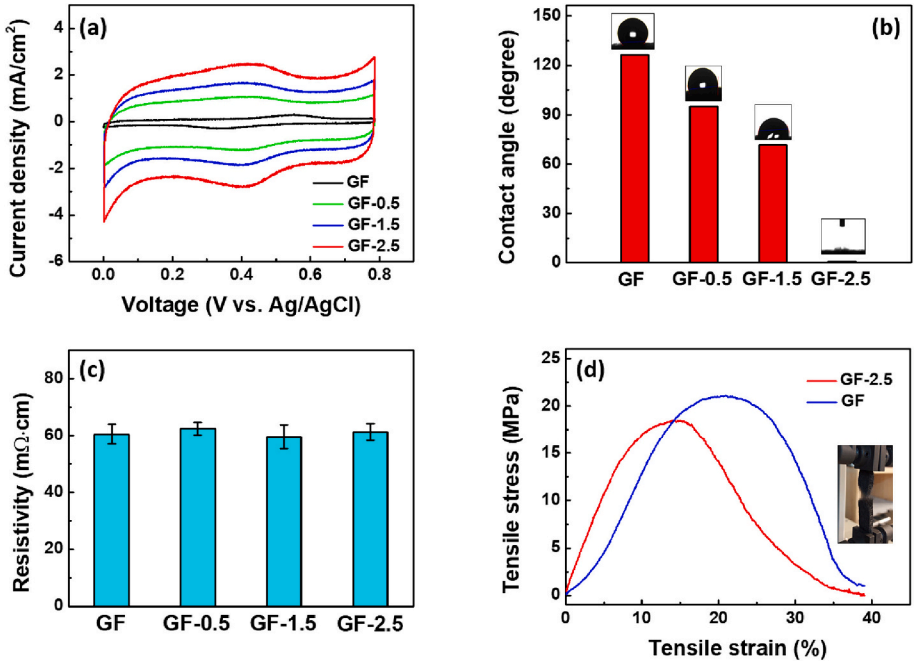

Fig. 5. The surface, electrical, and mechanical properties of the modified GF. (a) CV curve of the four samples in 1.0 M H_2SO_4 electrolyte with a scan rate of 1 mV/s; (b) the water contact angle of the pristine and modified GF with the corresponding images; (c) the resistivity measurement of the four samples and (d) the mechanical property of the pristine GF and GF-2.5.

However, the resistivity of the modified GF is almost unchanged compared with that of the pristine one (60.5 mΩ·cm). The constancy of conductivity can be attributed to the impact of nitrogen doping, which simultaneously enhances charge transfer without sacrificing the overall electrical conductivity [45,46]. In the VRFB design, flat sheets of graphite bipolar plates and GF electrodes generally are stacked without any bonding, which requires a certain degree of compression to minimize the contact resistance. If the mechanical strength is insufficient, it will affect the compression of the GF electrode, leading to non-uniform flow distribution and contact resistance. Fig. 5d shows the stress-strain curves for pristine GF and GF-2.5. The pristine displays a stress at break (21.05 MPa) with a strain of 20.8 %. In contrast, both the stress (18.37 MPa) and strain (14.8 %)of GF-2.5 at break become slightly smaller, indicating that the mechanical strength of GF-2.5 cannot be significantly altered after the modification.

To investigate the electrocatalytic activity towards the VO^{2+}/VO_2^+ redox couple, CV measurements of these samples were conducted using a three-electrode configuration in a 0.025 M VO^{2+}/2.0 M H_2SO_4 electrolyte. The CV curves of these GF electrodes tested at 1.0 mV/s are presented in Fig. 6a. It can be observed that the anodic and cathodic peak potential difference (ΔE) of the modified electrode is smaller than that of the pristine electrode, indicating the reduced mass transport and charge transfer resistances due to the better wettability and porous surface. A tiny peak at 0.65 V can be seen in the modified samples, which originated from the oxidation of TiO_2 [47]. Besides, the electrochemical polarization decreases with a larger content of urea, and the ΔE value of GF, GF-0.5, GF-1.5, and GF-2.5 electrodes are found to be 0.419, 0.335, 0.190, and 0.154 V, respectively (Fig. 6b). The CV curves of GF and GF-2.5 electrodes stepped at different scan rates are also displayed in Fig. 6c, d, respectively. The dependence of the anodic (I_a)/cathodic peak currents (I_c) on the square root of the scan rates ($\upsilon^{1/2}$) is presented in Fig. 6e. The linear relationship between the peak current and $\upsilon^{1/2}$, demonstrating that the corresponding redox reaction is diffusion-controlled. Moreover, the GF-2.5 electrode reveals a much steeper slope in both anodic and cathodic processes than that of the GF electrode. According to Randles-Sevcik relation [48], the larger slope of the GF-2.5 electrode signifies its faster ionic diffusion due to its porous structure and better electrolyte penetration. In addition, the ratios of the slopes obtained from the anodic and cathodic processes for GF and GF-2.5 electrodes are calculated to be 1.33 and 1.04, respectively. The GF-2.5 electrode, with a ratio closer to 1, suggests enhanced electrochemical reversibility. The EIS measurement was carried out further to support the excellent electrochemical behavior of modified GF electrodes as shown in Fig. 6f. The semicircle as shown in the Nyquist plot corresponds to charge transfer resistance (R_{ct}) caused by Faradaic reactions, which can be attributed to the VO^{2+}/VO_2^+ redox couple. The GF-2.5 electrode shows the smallest semicircle radius among these samples, indicating its low R_{ct} and rapid electrochemical kinetics. The comparison of impedance parameters obtained from the equivalent circuit model as shown in the inset of Fig. 6f is also provided in Table S1.

Fig. 7a, b show the charge-discharge profiles of the VRFB based on pristine and modified GFs with various current densities. Both the two VRFBs reveal a decrease in charging and discharging time with an increasing current density. Compared with the pristine GF-based VRFB, the GF-2.5-based battery delivers longer charge–discharge time at all current densities, indicating its higher discharged capacity and EE. In addition, a quick voltage loss (IR drop) can be noticed when the current is reversed from charging to discharging for all the charge-discharge curves, which originates from the internal resistance of the VRFB [49,50]. The internal resistance values can be evaluated from the slope of the relationship between the IR drop and the current density [51]. Fig. 7c exhibits the linear fitting dependence of IR drop on the applied current density for the two VRFBs. The GF-2.5-based VRFB shows a smaller slope than that of the pristine GF-based one, indicating its reduced internal resistance, which may be attributed to the unique structure and improved catalytic property of GF-2.5. The CE, VE, and EE values of VRFBs assembled with pristine GF and GF-2.5 at different current densities are compared as shown in Fig. 7d–f. It is evident that the two VRFBs show an increase in CE with higher current densities, primarily because it takes less time to reach an equivalent state of charge [52]. In contrast to CE, both VE and EE gradually decrease as the current density is increased, due to the higher ohmic loss associated with greater applied current densities [53]. It can be observed that the CE values of the two VRFBs are almost equal at the same current density owing to the identical electrolyte and membrane. In contrast, both the VE and EE values of the GF-2.5-based VRFB are higher than those of pristine GF-based cells at all current densities, especially at high current density. Furthermore, the VRFB incorporated with a GF-2.5 electrode can deliver a discharge capacity of 18.05 Ah/L at 160 mA/cm^2, which is 1.6 times larger than that of a GF-based cell (11.50 Ah/L) as shown in Fig. 7g. The smaller potential polarization observed in the GF-2.5-based VRFB is also in line with the IR drop observed in Fig. 7c. The discharge capacities of the two cells at different current densities are shown in Fig. 7h. The discharge capacity of GF-2.5 based cell is always higher than that of

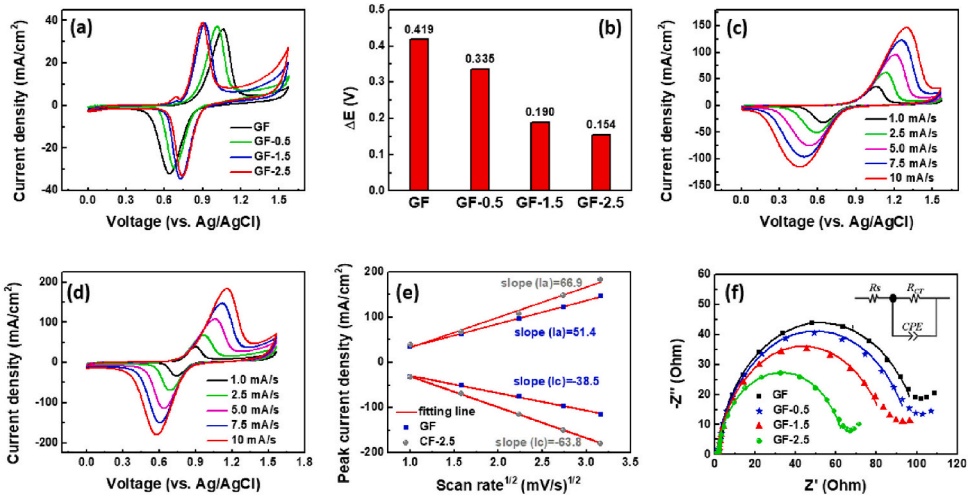

Fig. 6. The electrochemical property of the modified GF (a) CV curve of the pristine and modified GF with a scan rate of 1.0 mV/s; (b) the electrochemical polarization of the four samples; the CV curves of (c) pristine GF and (d) GF-2.5 with various scan rates; (e) the linear relationship of the anodic and cathodic peak current density and the square root of scan rate ($\upsilon^{1/2}$) and (f) Nyquist plots of the four samples with the equivalent circuit used to fit the EIS. *Rs*: electrolyte resistance; *R*ct: charge transfer resistance at electrode/electrolyte interface; CPE: double-layer capacitance at electrode/electrolyte interface.

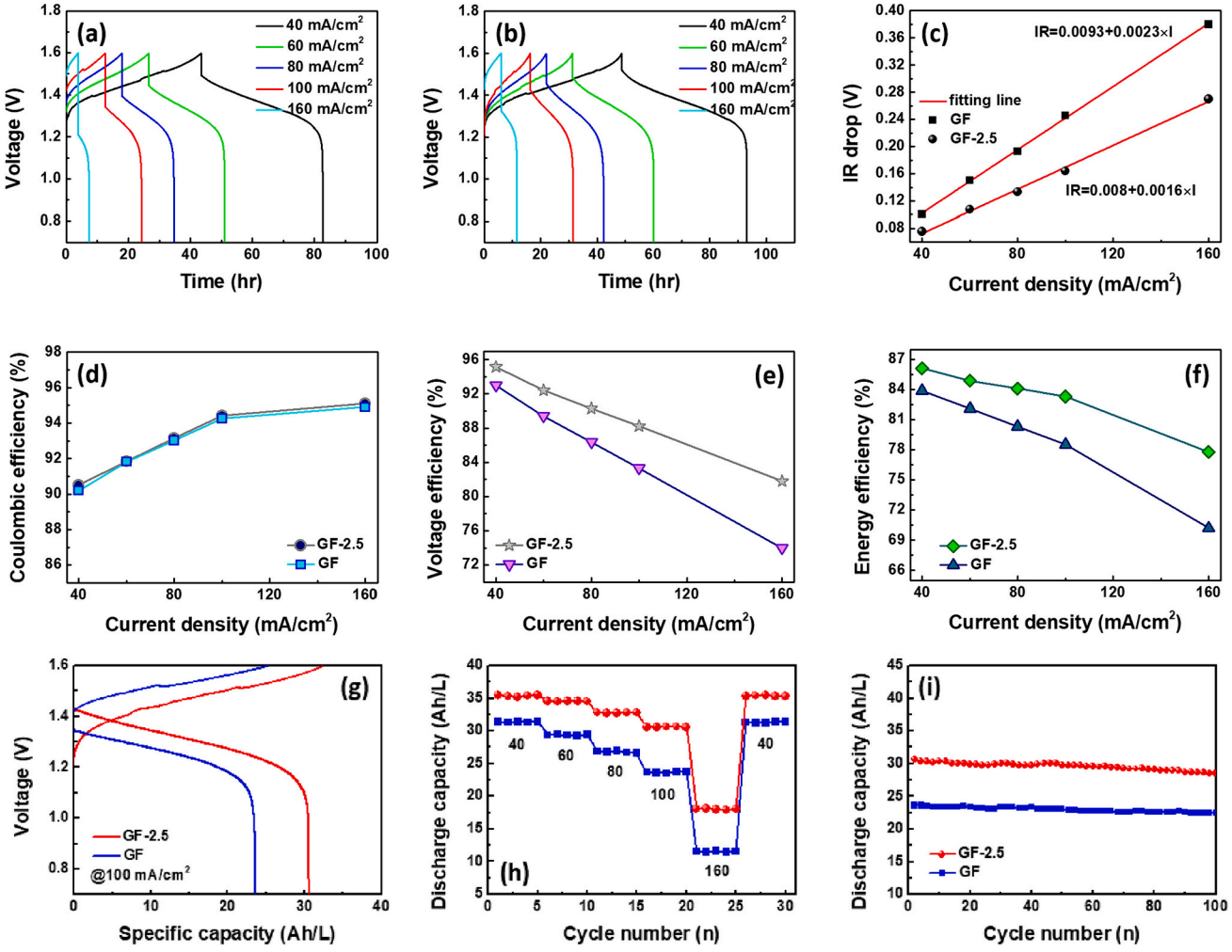

Fig. 7. Electrochemical performance of VRFB employing GF-2.5 electrode. The charge-discharge curves with various current densities of the VRFBs incorporated with (a) GF and (b) GF-2.5 electrodes; (c) the linear fitting dependence of IR drop on the applied current density for the two VRFBs; (d) coulombic efficiency (CE); (e) voltage efficiency (VE) and (f) energy efficiency (EE) of the two VRFBs at different current densities; (g) the charge-discharge curve of the two VRFBs at 100 mA/cm^2; (h) the discharged capacity of the two VRFBs at different current densities and (i) cycling stability of the two VRFBs tested at 100 mA/cm^2.

pristine GF based one and the difference in capacity becomes more pronounced at higher current density, indicating the improved rate capability of the GF-2.5 based cell. The comparison of modified GF with other metal oxides in the application of VRFB is also provided in Table S2. The effect of the surface modification on the durability was also evaluated and the results are presented in Fig. 7i. After 100 cycles at 100 mA/cm^2, the capacity retentions of the pristine and modified GF-based VRFBs are found to be 94.4 % and 93.5 %, respectively, suggesting that the surface modification does not significantly affect cycling stability. These findings imply that the combined impact of surface modification with TiO_2, the porous structure, nitrogen doping, and the introduction of oxygen defects on the GF can efficiently facilitate mass transport, accelerate charge transfer, and improve the utilization of the vanadium electrolyte. This, in turn, results in enhanced EE, rate capability, and discharge capacity. The cycling stability of the modified GF-based VRFB with 200 cycles is also shown in Fig. S4.

4. Conclusion

In summary, the modified GF electrodes with a synergistic effect of porous surfaces, TiO_2 decoration, and incorporation of defects were synthesized. The modified GF possesses superior electrochemical kinetics and reversibility because of its porous and hydrophilic surface enhancing the electrolyte penetration and ion diffusion. Moreover, the abundant oxygen-containing functional groups with nitrogen doping and decorated TiO_2 particles also provide plentiful electrocatalytic sites for the VO^{2+}/VO_2^+ redox couple. The as-assembled VRFB using the modified GF electrode shows a remarkable energy efficiency of 77.8 % at a current density of 160 mA/cm^2. Additionally, the VRFB also delivers superior cycling stability with 93.5 % retention after 100 cycles at 100 mA/cm^2. These results demonstrate that the strategy we have proposed is highly efficient for the development of modified GF towards high-performance VRFB.

CRediT authorship contribution statement

Yu-Sheng Hsiao: Writing – review & editing, Writing – original draft, Supervision, Project administration, Investigation, Conceptualization. **Jen-Hsien Huang:** Writing – original draft, Methodology, Investigation, Formal analysis, Data curation. **Hong-Yu Lin:** Methodology, Formal analysis, Data curation. **Wei Kong Pang:** Formal analysis, Data curation. **Min-Tzu Hung:** Formal analysis, Data curation. **Ta-Hung Cheng:** Data curation. **Shih-Chieh Hsu:** Supervision. **Huei Chu Weng:** Resources. **Yu-Ching Huang:** Supervision, Resources.

Declaration of competing interest

The authors declare that they have no known competing financial

interests or personal relationships that could have appeared to influence the work reported in this paper.

Acknowledgment

We are grateful to the National Science and Technology Council (NSTC) of Taiwan (grant no.: MOST 111-2628-E-011-003-MY2) for financial support.

Appendix A. Supplementary data

Supplementary data to this article can be found online at https://doi.org/10.1016/j.surfcoat.2024.130785.

References

[1] A.G. Olabi, C. Onumaegbu, T. Wilberforce, M. Ramadan, M.A. Abdelkareem, A. H. Al-Alami, Critical review of energy storage systems, Energy 214 (2021) 118987.
[2] H. Chen, T.N. Cong, W. Yang, C. Tan, Y. Li, Y. Ding, Progress in electrical energy storage system: a critical review, Prog. Nat. Sci. 19 (2009) 291–312.
[3] H. Ibrahim, A. Ilinca, J. Perron, Energy storage systems-characteristics and comparisons, Renew. Sustain. Energy Rev. 12 (2008) 1221–1250.
[4] M. Skyllas-Kazacos, M. Rychcik, R.G. Robins, A.G. Fane, M.A. Green, New all-vanadium redox flow cell, J. Electrochem. Soc. 133 (1986) 1057.
[5] M. Skyllas-Kazacos, F. Grossmith, Efficient vanadium redox flow cell, J. Electrochem. Soc. 134 (1987) 2950.
[6] M. Skyllas-Kazacos, M.H. Chakrabarti, S.A. Hajimolana, F.S. Mjalli, M. Saleem, Progress in flow battery Research and Development, J. Electrochem. Soc. 158 (2011) R55.
[7] P.C. Ghimire, R. Schweiss, G.G. Scherer, N. Wai, T.M. Lim, A. Bhattarai, T. D. Nguyen, Q. Yan, Titanium carbide-decorated graphite felt as high performance negative electrode in vanadium redox flow batteries, J. Mater. Chem. A 6 (2018) 6625–6632.
[8] X. Wu, H. Xu, Y. Shen, P. Xu, L. Lu, J. Fu, H. Zhao, Treatment of graphite felt by modified hummers method for the positive electrode of vanadium redox flow battery, Electrochim. Acta 138 (2014) 264–269.
[9] J. Xu, Y. Zhang, Z. Huang, C. Jia, S. Wang, Surface modification of carbon-based electrodes for vanadium redox flow batteries, Energy Fuel 35 (2021) 8617–8633.
[10] H.R. Jiang, W. Shyy, L. Zeng, R.H. Zhang, T.S. Zhao, Highly efficient and ultra-stable boron-doped graphite felt electrodes for vanadium redox flow batteries, J. Mater. Chem. A 6 (2018) 13244–13253.
[11] M. Park, J. Ryu, J. Cho, Nanostructured electrocatalysts for all-vanadium redox flow batteries, Chem. Asian J. 10 (2015) 2096–2110.
[12] Y. Jiang, Z. Liu, Y. Lv, A. Tang, L. Dai, L. Wang, Z. He, Perovskite enables high performance vanadium redox flow battery, Chem. Eng. J. 443 (2022) 136341.
[13] Q. Jiang, Y. Ren, Y. Yang, H. Liu, L. Wang, J. Li, L. Dai, Z. He, High-activity and stability graphite felt supported by Fe, N, S co-doped carbon nanofibers derived from bimetal-organic framework for vanadium redox flow battery, Chem. Eng. J. 460 (2023) 141751.
[14] Y. Jiang, G. Cheng, Y. Li, Z. He, J. Zhu, W. Meng, L. Dai, L. Wang, Promoting vanadium redox flow battery performance by ultra-uniform ZrO_2@C from metal-organic framework, Chem. Eng. J. 415 (2021) 129014.
[15] Q.C. Jiang, J. Li, Y.J. Yang, Y.J. Ren, L. Dai, J.Y. Gao, L. Wang, J.Y. Ye, Z.X. He, Ultrafine SnO_2 in situ modified graphite felt derived from metal–organic framework as a superior electrode for vanadium redox flow battery, Rare Metals 42 (2023) 1214–1226.
[16] Y.C. Chang, Y.C. Shih, J.Y. Chen, G.Y. Lin, N.Y. Hsu, Y.S. Chou, C.H. Wang, High efficiency of bamboo-like carbon nanotube on functionalized graphite felt as electrode in vanadium redox flow battery, RSC Adv. 6 (2016) 102068–102075.
[17] D.M. Kabtamu, J.-Y. Chen, Y.C. Chang, C.H. Wang, Electrocatalytic activity of Nb-doped hexagonal WO_3 nanowire-modified graphite felt as a positive electrode for vanadium redox flow batteries, J. Mater. Chem. A 4 (2016) 11472–11480.
[18] D.S. Yang, J.H. Han, J.W. Jeon, J.Y. Lee, D.G. Kim, D.H. Seo, B.G. Kim, T.H. Kim, Y. T. Hong, Multimodal porous and nitrogen-functionalized electrode based on graphite felt modified with carbonized porous polymer skin layer for all-vanadium redox flow battery, Mater. Today Energy 11 (2019) 159–165.
[19] J. Ji, C. Noh, M. Shin, S. Oh, Y. Chung, Y. Kwon, D.H. Kim, Vanadium redox flow batteries using new mesoporous nitrogen-doped carbon coated graphite felt electrode, Appl. Surf. Sci. 611 (2023) 155665.
[20] J.J. Park, J.H. Park, O.O. Park, J.H. Yang, Highly porous graphenated graphite felt electrodes with catalytic defects for highperformance vanadium redox flow batteries produced via NiO/Ni redox reactions, Carbon 110 (2016) 17–26.
[21] L. Zhang, J. Yue, Q. Deng, W. Ling, C.J. Zhou, X.X. Zeng, C. Zhou, X.W. Wu, Y. P. Wu, Preparation of a porous graphite felt electrode for advance vanadium redox flow batteries 10 (2020) 13374–13378.
[22] T. Ličko, V. Figusch, J. Púichyová, Carbothermal reduction and nitriding of TiO_2, J. Eur. Ceram. Soc. 5 (1989) 257–265.
[23] Y. Gao, Q. Wang, G. Ji, A. Li, J. Niu, Doping strategy, properties and application of heteroatom-doped ordered mesoporous carbon, RSC Adv. 11 (2021) 5361–5383.
[24] Z. Qiu, K. Zhao, J. Liu, S. Xia, Nitrogen-doped mesoporous carbon as an anode material for high performance potassium-ion batteries, Electrochim. Acta 340 (2020) 135947.
[25] L. Zhang, Z.G. Shao, X. Wang, H. Yu, S. Liu, B. Yi, The characterization of graphite felt electrode with surface modification for H_2/Br_2 fuel cell, J. Power Sources 242 (2013) 15–22.
[26] M. Asif, M. Zafar, P. Akhter, M. Hussain, A. Umer, A. Razzaq, W.Y. Kim, Effect of urea addition on anatase phase enrichment and nitrogen doping of TiO_2 for photocatalytic abatement of methylene blue, Appl. Sci. 11 (2021) 8264.
[27] H. Lin, L. Li, M. Zhao, X. Huang, X. Chen, G. Li, R. Yu, Synthesis of high-quality brookite TiO_2 single-crystalline nanosheets with specific facets exposed: tuning catalysts from inert to highly reactive, J. Am. Chem. Soc. 134 (2012) 8328–8331.
[28] S. Challagulla, K. Tarafder, R. Ganesan, S. Roy, Structure sensitive photocatalytic reduction of nitroarenes over TiO_2, Sci. Rep. 7 (2017) 8783.
[29] U. Balachandran, N.G. Eror, Raman spectra of titanium dioxide, J. Solid State Chem. 42 (1982) 276–282.
[30] G.C. Vásquez, D. Maestre, A. Cremades, J. Piqueras, Assessment of the Cr doping and size effects on the Raman-active modes of rutile TiO_2 by UV/visible polarized Raman spectroscopy, J. Raman Spectrosc. 48 (2017) 847–854.
[31] Z. Xu, H. Xu, Z. Hu, W. Wu, J. Xu, F. Zhong, M. Ding, X. Zhu, H. Fu, C. Jia, Carbon felt decorated with carbon derived from spent asphalt as a low-cost and high-performance electrode for vanadium redox flow batteries, ChemNanoMat 8 (2022) e202200027.
[32] N.A. Almeida, P.M. Martins, S. Teixeira, J.A. Lopes da Silva, V. Sencadas, K. Kühn, G. Cuniberti, S. Lanceros-Mendez, P.A.A.P. Marques, TiO_2/graphene oxide immobilized in P(VDF-TrFE) electrospun membranes with enhanced visible-lightinduced photocatalytic performance, J. Mater. Sci. 51 (2016) 6974–6986.
[33] T. Wu, K. Huang, S. Liu, S. Zhuang, D. Fang, S. Li, D. Lu, A. Su, Hydrothermal ammoniated treatment of PAN-graphite felt for vanadium redox flow battery, J. Solid State Electrochem. 16 (2012) 579–585.
[34] Y.L. Yao, Y. Ding, L.S. Ye, X.H. Xia, Two-step pyrolysis process to synthesize highly dispersed Pt–Ru/carbon nanotube catalysts for methanol electrooxidation, Carbon 44 (2006) 61–66.
[35] Y.H. Wang, I.M. Hung, C.Y. Wu, V_2O_5-activated graphite felt with enhanced Aactivity for vanadium redox flow battery, Catalysts 11 (2021) 800.
[36] R.U. Soni, V.A. Edlabadkar, D. Greenan, P.M. Rewatkar, N. Leventis, C. Sotiriou-Leventis, Preparation of carbon aerogels from polymer-cross-linked xerogel powders without supercritical fluid drying and their application in highly selective CO_2 adsorption, Chem. Mater. 34 (2022) 4828–4847.
[37] B. Sivaranjini, R. Mangaiyarkarasi, V. Ganesh, S. Umadevi, Vertical alignment of liquid crystals over a functionalized flexible substrate, Sci. Rep. 8 (2018) 8891.
[38] X. Zhang, Q. Fan, N. Qu, H. Yang, M. Wang, A. Liu, J. Yang, Ultrathin 2D nitrogen-doped carbon nanosheetsfor high performance supercapacitors: insight into the effects of graphene oxides, Nanoscale 11 (2019) 8588–8596.
[39] J.Y. Lee, N.Y. Kim, D.Y. Shin, H.Y. Park, S.S. Lee, S.J. Kwon, D.H. Lim, K.W. Bong, J.G. Son, J.Y. Kim, Nitrogen-doped graphene-wrapped iron nanofragments for high-performance oxygen reduction electrocatalysts, J. Nanopart. Res. 19 (2017) 98.
[40] H. Song, T.G. Jeong, Y.H. Moon, H.H. Chun, K.Y. Chung, H.S. Kim, B.W. Cho, Y. T. Kim, Stabilization of oxygen-deficient structure for conducting $Li_4Ti_5O_{12-\delta}$ by molybdenum doping in a reducing atmosphere, Sci. Rep. 4 (2014) 4350.
[41] J.Y. Shin, J.H. Joo, D. Samuelis, J. Maier, Oxygen-deficient $TiO_{2-\delta}$ nanoparticles via hydrogen reduction for high rate capability lithium batteries, Chem. Mater. 24 (2012) 543–551.
[42] S.J. Yoon, S. Kim, D.K. Kim, S. So, Y.T. Hong, R. Hempelmann, Ionic liquid derived nitrogen doped graphite felt electrodes for vanadium redox flow batteries, Carbon 166 (2020) 131–137.
[43] A. Mukhopadhyay, Y. Yang, Y. Li, Y. Chen, H. Li, A. Natan, Y. Liu, D. Cao, H. Zhu, Mass transfer and reaction kinetic enhanced electrode for high-performance aqueous flow batteries, Adv. Funct. Mater. 29 (2019) 1903192.
[44] J. Vázquez-Galván, C. Flox, C. Fàbrega, E. Ventosa, A. Parra, T. Andreu, J. R. Morante, Hydrogen treated rutile TiO_2 shell in graphite core structure as a negative electrode for high-performance vanadium flow batteries, ChemSusChem 10 (2017) 2089–2098.
[45] Q. Yang, W. Xu, A. Tomita, T. Kyotani, Double coaxial structure and dual physicochemical properties of carbon nanotubes composed of stacked nitrogen-doped and undoped multiwalls, Chem. Mater. 17 (2005) 2940–2945.
[46] Y. Zhou, K. Neyerlin, T.S. Olson, S. Pylypenko, J. Bult, H.N. Dinh, T. Gennett, Z. Shao, R. O'Hayre, Enhancement of Pt and Pt-alloy fuel cell catalyst activity and durability via nitrogen-modified carbon supports, Energ. Environ. Sci. 3 (2010) 1437–1446.
[47] B. Vidyadharan, P.S. Archana, J. Ismail, M.M. Yusoff, R. Jose, Improved supercapacitive charge storage in electrospun niobium doped titania nanowires, RSC Adv. 5 (2015) 50087–50097.
[48] Z.T. Liu, T.H. Hsieh, C.W. Huang, M.L. Lee, W.R. Liu, Temperature effects on hard carbon derived from sawdust as anode materials for sodium ion batteries, J. Taiwan Inst. Chem. Eng. 5 (2023) 104889.
[49] S. Jeong, S. Kim, Y. Kwon, Performance enhancement in vanadium redox flow battery using platinum-based electrocatalyst synthesized by polyol process, Electrochim. Acta 114 (2013) 439–447.
[50] T.M. Tseng, R.H. Huang, C.Y. Huang, C.C. Liu, K.L. Hsueh, F.S. Shieu, Carbon felt coated with titanium dioxide/carbon black composite as negative electrode for vanadium redox flow battery, J. Electrochem. Soc. 161 (2014) A1132.

[51] J.G. Wang, Y. Yang, Z.H. Huang, F. Kang, A high-performance asymmetric supercapacitor based on carbon and carbon–MnO2 nanofiber electrodes, Carbon 61 (2013) 190–199.
[52] Y. Li, J. Sniekers, J.C. Malaquias, C.V. Goethem, K. Binnemans, J. Fransaer, I.F. J. Vankelecom, Crosslinked anion exchange membranes prepared from poly (phenylene oxide) (PPO) for non-aqueous redox flow batteries, J. Power Sources 378 (2018) 338–344.
[53] S.S. Sha'rani, N.W.C. Jusoh, E. Abouzari-Lotf, A. Ahmad, R.R. Ali, Evaluation of perfluorinated sulfonic acid membranes for vanadium redox, IOP Conf. Ser.: Mater. Sci. Eng. 808 (2020) 012026.